Dutcher,[22] Emilio Fernández,[23] Patrick Ferris,[15] Hideya Fukuzawa,[24] David González-Ballester,[17] Diego González-Halphen,[25] Armin Hallmann,[26] Marc Hanikenne,[18] Michael Hippler,[27] William Inwood,[21] Kamel Jabbari,[28] Ming Kalanon,[29] Richard Kuras,[3] Paul A. Lefebvre,[11] Stéphane D. Lemaire,[30] Alexey V. Lobanov,[31] Martin Lohr,[32] Andrea Manuell,[33] Iris Meier,[34] Laurens Mets,[35] Maria Mittag,[36] Telsa Mittelmeier,[37] James V. Moroney,[38] Jeffrey Moseley,[17] Carolyn Napoli,[39] Aurora M. Nedelcu,[40] Krishna Niyogi,[21] Sergey V. Novoselov,[31] Ian T. Paulsen,[14] Greg Pazour,[41] Saul Purton,[42] Jean-Philippe Ral,[43] Diego Mauricio Riaño-Pachón,[44] Wayne Riekhof,[45] Linda Rymarquis,[46] Michael Schroda,[47] David Stern,[48] James Umen,[15] Robert Willows,[49] Nedra Wilson,[50] Sara Lana Zimmer,[48] Jens Allmer,[51] Janneke Balk,[20] Katerina Bisova,[52] Chong-Jian Chen,[9] Marek Elias,[53] Karla Gendler,[39] Charles Hauser,[54] Mary Rose Lamb,[55] Heidi Ledford,[21] Joanne C. Long,[1] Jun Minagawa,[56] M. Dudley Page,[1] Junmin Pan,[57] Wirulda Pootakham,[17] Sanja Roje,[58] Annkatrin Rose,[59] Eric Stahlberg,[34] Aimee M. Terauchi,[1] Pinfen Yang,[60] Steven Ball,[61] Chris Bowler,[28,62] Carol L. Dieckmann,[37] Vadim N. Gladyshev,[31] Pamela Green,[46] Richard Jorgensen,[39] Stephen Mayfield,[33] Bernd Mueller-Roeber,[44] Sathish Rajamani,[63] Richard T. Sayre[34]

JGI Annotation Team. Peter Brokstein,[2] Inna Dubchak,[2] David Goodstein,[2] Leila Hornick,[2] Y. Wayne Huang,[2] Jinal Jhaveri,[2] Yigong Luo,[2] Diego Martínez,[2] Wing Chi Abby Ngau,[2] Bobby Otillar,[2] Alexander Poliakov,[2] Aaron Porter,[2] Lukasz Szajkowski,[2] Gregory Werner,[2] Kemin Zhou[2]

[1]Department of Chemistry and Biochemistry, University of California Los Angeles, Los Angeles, CA 90095, USA. [2]U.S. Department of Energy, Joint Genome Institute, Walnut Creek, CA 94598, USA. [3]CNRS, UMR 7141, CNRS/Université Paris 6, Institut de Biologie Physico-Chimique, 75005 Paris, France. [4]Department of Biology, Duke University, Durham, North Carolina 27708, USA. [5]Department of Cell Biology, University of Massachusetts Medical School, Worcester, MA 01655, USA. [6]Department of Molecular and Cell Biology, University of California at Berkeley, Berkeley, CA94720, USA. [7]Institut de Biologie Moléculaire des Plantes, CNRS, 67084 Strasbourg Cedex, France. [8]Department of Biochemistry and Biophysics, University of California at San Francisco, San Francisco, CA 94143, USA. [9]Biotechnology Research Center, Zhongshan University, Guangzhou 510275, China. [10]Department of Molecular Sciences and Center of Excellence in Genomics and Bioinformatics, University of Tennessee, Memphis, TN 38163, USA. [11]Department of Plant Biology, University of Minnesota, St. Paul MN 55108, USA. [12]Department of Genetics, Development, and Cell Biology, Iowa State University, Ames, IA 50011, USA. [13]Genetic Information Research Institute, Mountain View, CA 94043, USA. [14]The Institute for Genomic Research, Rockville, MD 20850, USA. [15]Plant Biology Laboratory, Salk Institute, La Jolla, CA 92037, USA. [16]Stanford Human Genome Center, Stanford University School of Medicine, Palo Alto, CA 94304, USA. [17]Department of Plant Biology, Carnegie Institution, Stanford, CA 94306, USA. [18]Plant Biology Institute, Department of Life Sciences, University of Liège, B-4000 Liège, Belgium. [19]University of Nebraska-Lincoln, School of Biological Sciences–Plant Science Initiative, Lincoln, NE 68588, USA. [20]Department of Plant Sciences, University of Cambridge, Cambridge CB2 3EA, UK. [21]Department of Plant and Microbial Biology, University of California at Berkeley, Berkeley, CA 94720, USA. [22]Department of Genetics, Washington University School of Medicine, St. Louis, MO 63110, USA. [23]Departamento de Bioquímica y Biología Molecular, Facultad de Ciencias, Universidad de Córdoba, Campus de Rabanales, 14071 Córdoba, Spain. [24]Graduate School of Biostudies, Kyoto University, Kyoto 606-8502, Japan. [25]Departamento de Genética Molecular, Instituto de Fisiología Celular, Universidad Nacional Autónoma de México, México 04510 DF, Mexico. [26]Department of Cellular and Developmental Biology of Plants, University of Bielefeld, D-33615 Bielefeld, Germany. [27]Department of Biology, Institute of Plant Biochemistry and Biotechnology, University of Münster, 48143 Münster, Germany. [28]CNRS UMR 8186, Département de Biologie, Ecole Normale Supérieure, 75230 Paris, France. [29]Plant Cell Biology Research Centre, The School of Botany, The University of Melbourne, Parkville, Melbourne, VIC 3010, Australia. [30]Institut de Biotechnologie des Plantes, UMR 8618, CNRS/Université Paris-Sud, Orsay, France. [31]Department of Biochemistry, N151 Beadle Center, University of Nebraska, Lincoln, NE 68588–0664, USA. [32]Institut für Allgemeine Botanik, Johannes Gutenberg-Universität, 55099 Mainz, Germany. [33]Department of Cell Biology and Skaggs Institute for Chemical Biology, Scripps Research Institute, La Jolla, CA 92037, USA. [34]PCMB and Plant Biotechnology Center, Ohio State University, Columbus, OH 43210, USA. [35]Molecular Genetics and Cell Biology, University of Chicago, Chicago, IL 60637, USA. [36]Institut für Allgemeine Botanik und Pflanzenphysiologie, Friedrich-Schiller-Universität Jena, 07743 Jena, Germany. [37]Department of Molecular and Cellular Biology, University of Arizona, Tucson, AZ 85721, USA. [38]Department of Biological Science, Louisiana State University, Baton Rouge, LA 70803, USA. [39]Department of Plant Sciences, University of Arizona, Tucson, AZ 85721, USA. [40]Department of Biology, University of New Brunswick, Fredericton, NB, Canada E3B 6E1. [41]Department of Physiology, University of Massachusetts Medical School, Worcester, MA 01605, USA. [42]Department of Biology, University College London, London WC1E 6BT, UK. [43]Unité de Glycobiologie Structurale et Fonctionnelle, UMR8576 CNRS/USTL, IFR 118, Université des Sciences et Technologies de Lille, Cedex, France. [44]Universität Potsdam, Institut für Biochemie und Biologie, D-14476 Golm, Germany. [45]Department of Medicine, National Jewish Medical and Research Center, Denver, CO 80206, USA. [46]Delaware Biotechnology Institute, University of Delaware, Newark, DE 19711, USA. [47]Institute of Biology II/Plant Biochemistry, 79104 Freiburg, Germany. [48]Boyce Thompson Institute for Plant Research at Cornell University, Ithaca, NY 14853, USA. [49]Department of Chemistry and Biomolecular Sciences, Macquarie University, Sydney 2109, Australia. [50]Department of Anatomy and Cell Biology, Oklahoma State University, Center for Health Sciences, Tulsa, OK 74107, USA. [51]Izmir Ekonomi Universitesi, 35330 Balcova-Izmir Turkey. [52]Institute of Microbiology, Czech Academy of Sciences, Czech Republic. [53]Department of Plant Physiology, Faculty of Sciences, Charles University, 128 44 Prague 2, Czech Republic. [54]Bioinformatics Program, St. Edward's University, Austin, TX 78704, USA. [55]Department of Biology, University of Puget Sound, Tacoma, WA 98407, USA. [56]Institute of Low-Temperature Science, Hokkaido University, 060-0819, Japan. [57]Department of Biology, Tsinghua University, Beijing, China 100084. [58]Institute of Biological Chemistry, Washington State University, Pullman, WA 99164, USA. [59]Appalachian State University, Boone, NC 28608, USA. [60]Department of Biology, Marquette University, Milwaukee, WI 53233, USA. [61]UMR8576 CNRS, Laboratory of Biological Chemistry, 59655 Villeneuve d'Ascq, France. [62]Cell Signaling Laboratory, Stazione Zoologica, I 80121 Naples, Italy. [63]Graduate Program in Biophysics, Ohio State University, Columbus, OH 43210, USA.

Supporting Online Material
www.sciencemag.org/cgi/content/full/318/5848/245/DC1
Materials and Methods
SOM Text
Figs. S1 to S25
Tables S1 to S14
References and Notes

9 April 2007; accepted 5 September 2007
10.1126/science.1143609

REPORTS

Dislocation Avalanches, Strain Bursts, and the Problem of Plastic Forming at the Micrometer Scale

Ferenc F. Csikor,[1,2] Christian Motz,[3] Daniel Weygand,[3] Michael Zaiser,[2] Stefano Zapperi[4,5]*

Under stress, many crystalline materials exhibit irreversible plastic deformation caused by the motion of lattice dislocations. In plastically deformed microcrystals, internal dislocation avalanches lead to jumps in the stress-strain curves (strain bursts), whereas in macroscopic samples plasticity appears as a smooth process. By combining three-dimensional simulations of the dynamics of interacting dislocations with statistical analysis of the corresponding deformation behavior, we determined the distribution of strain changes during dislocation avalanches and established its dependence on microcrystal size. Our results suggest that for sample dimensions on the micrometer and submicrometer scale, large strain fluctuations may make it difficult to control the resulting shape in a plastic-forming process.

In recent years, experimental evidence has accumulated that indicates that plastic flow is—at least on the micrometer scale—characterized by intermittent strain bursts with scale-free (i.e, power-law) size distributions (*1*–*8*). The phenomenology of these strain bursts closely resembles that of macroscopic plastic instabilities: Stress-strain curves are characterized by serrated yielding under displacement control and assume a staircase shape under conditions of stress control. Temporal intermittency is associated with spatial localization because each strain burst corresponds to the formation of a narrow slip line or slip band (*9*). On the macroscopic scale, spatiotemporal localization of plastic deformation associated with plastic instabilities is well known to have a detrimental effect on formability. A classic example is the strain bursts discovered by Portevin and le Chatelier (PLC effect), which arise from the interaction between dislocations and diffusing solutes (*10*). The PLC effect limits the applicability of many aluminum alloys in sheet metal–forming processes, but only arises under specific deformation conditions. Thus, the instability can be circumvented by appropriately choosing the process path, avoiding those temperature and strain rate regimes in which the dislocation and solute velocities are of the same order of magnitude.

Here, we demonstrate that the burstlike deformation of microcrystals represents a much more fundamental instability of plastic flow that could cause intrinsic problems in the plastic forming of micrometer-size crystals. Strain bursts in microcrystals arise from the collective, avalanche-like motion of dislocations. The constraints to their motion imposed by the crystal lattice structure give dislocations the ability to mutually trap each other into jammed configurations. The long-range mutual interactions between dislocations make the destruction of such jammed configurations a collective, avalanche-like process. Because their occurrence depends only on the most basic features of dislocation plasticity, dislocation avalanches are a universal feature that does not depend on specific materials properties and cannot be avoided by adjusting the deformation path as in the PLC effect. Similar to other crackling noise phenomena (*11*) observed in driven systems, such as the Barkhausen noise emitted along the hysteresis loop in ferromagnets (*12*) or ferroelectrics (*13*), the acoustic emission during fracture (*14*, *15*), or the seismic activity during earthquakes, dislocation avalanches are characterized by material-independent power-law size distributions. Although the existence of intermittent plastic strain bursts has been known for many years (*16*–*18*), a statistical characterization was performed only recently by acoustic emission (AE) experiments in single slip deformation of hexagonal ice (*3*) or hexagonal close-packed metals (*8*), as well as by direct observation of strain bursts during deformation of micropillars (*2*). AE experiments, in particular, record the acoustic energy released during a burst and find power-law distributions of AE energies that do not exhibit any apparent cut-off (*3*–*6*). These observations raise several intriguing questions: What are the minimum "ingredients" required to produce dislocation avalanches, and are the avalanche properties truly universal? If there is no intrinsic limit to the magnitude of dislocation avalanches, why do we not see them in deformation curves of macroscopic samples? Or, if there is an intrinsic limit, why do we not see such a limit in AE measurements on macroscopic samples?

To resolve these issues, we investigate the dynamic behavior of dislocation systems under various loading conditions. To this end, we simulate the deformation of monocrystalline specimens using three-dimensional discrete dislocation dynamics. The model, described in detail in (*19*), considers an assembly of dislocation lines in a block made of a face-centered cubic metal (we use materials parameters of Al). Most of our simulations consider uniaxial tension/compression of cube-shaped specimens. Deformation is driven either by controlling the axial displacement of the top face of the cube (displacement control) or by slowly increasing the total force acting on the top face (load control) (*20*, *21*). In addition, we simulate the compression of bicrystals and multicrystals of various sizes, as well as the bending of a monocrystalline beam (aspect ratio 3:1:1) that is cantilevered in a cube orientation and deformed by imposing a downward displacement on its free end. In the compression simulations, we record the plastic strain $\varepsilon_{\mathrm{pl}}$ as well as the average stress (force per unit area acting on the top surface of the block). In the case of bending, we record the maximum bending stress and surface strain, from which we deduce a "plastic" bending strain by subtracting the surface strain of a purely elastic beam under the same bending moment.

An example of a typical stress-strain curve recorded in a load-controlled compression test is shown in Fig. 1. The staircase character of the response is very similar to that of the experimental observations in micrometer-sized samples (*2*). By differentiating the plastic strain versus time signal, we obtain the strain rate shown in the inset of Fig. 1. This is a typical example of a crackling noise signal, consisting of intermittent bursts with widely fluctuating amplitudes (*11*). These bursts arise from the propagation of dislocation avalanches within the sample. Dislocation activity during an avalanche is usually dominated by a single-slip system, even if deformation proceeds, on average, in symmetrical multiple slip. Consequently, the avalanches exhibit a characteristic lamellar shape, as shown in Fig. 2.

To analyze the crackling noise signal, we first threshold it to eliminate effects coming from numerical noise, and then identify well-defined pulses. The area s under each pulse is equivalent to the plastic strain increment produced by a dislocation avalanche (the avalanche strain). In analogy with experimental measurements that use multiple samples, we determine avalanche strain distributions $P(s)$ from multiple simulations with different, but statistically equivalent, initial configurations. Avalanches in bending deformation are analyzed in an analogous manner by considering the evolution of the plastic bending strain. In either case, the avalanche strain distributions have the general form

$$P(s) = C\, s^{-\tau} \exp[-(s/s_0)^2] \qquad (1)$$

where C is a normalization constant, τ is a scaling exponent, and s_0 is the characteristic strain of the largest avalanches.

To test the robustness of Eq. 1 in various physical situations, we compare distributions of avalanche strains for compression simulations performed in load control and displacement control, with and without activation of cross slip, in single slip and in multiple slip conditions. The avalanche strain distributions are essentially insensitive to the slip geometry and to the presence or absence of cross slip (Fig. 3 and figs. S1 and S2). In either case, the distributions can be described by Eq. 1 with $\tau \cong 1.5$. The same is true for the bending simulations. A very similar exponent was also reported in the experiment (*2*). In addition, the mean-field value $\tau = 3/2$ was predicted to hold for single-slip conditions in general by the theory of the dislocation yielding transition (*22*, *23*). Our simulations demonstrate that the universality of the exponent extends also to multiple-slip conditions and to deformation modes such as bending, which impose strain gradients on the sample scale. The last finding is particularly interesting because it demonstrates that the accumulation of "geometrically necessary" excess dislocations that is characteristic of inhomogeneous deformation processes does not change the statistical characteristics of dislocation avalanches.

To elucidate the physical origin of the cut-off, we consider the proposition (*22*, *23*) that during the progress of an avalanche, two processes reduce the effective stress acting upon the dislocations: (i) Because of intrinsic hardening with strain hardening coefficient Θ, a higher driving stress is needed to sustain the avalanche; and (ii) in case of

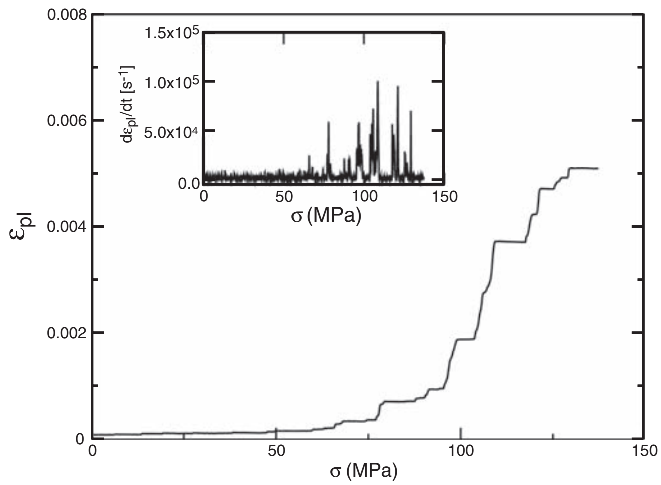

Fig. 1. A typical stress-strain curve obtained from simulation of the three-dimensional dislocation dynamics model in a load-controlled test in multiple-slip conditions. (**Inset**) The strain-rate signal displays the characteristics typical of crackling noise: bursts of activity of widely distributed amplitudes followed by more quiescent periods.

[1]Department of Materials Physics, Eötvös University, Post Office Box 32, H-1518 Budapest, Hungary. [2]Center for Materials Science and Engineering, University of Edinburgh, King's Buildings, Sanderson Building, Edinburgh EH93JL, UK. [3]Universität Karlsruhe, Institut für die Zuverlässigkeit von Bauteilen und Systemen, Kaiserstrasse 12, 76131 Karlsruhe, Germany. [4]Consiglio Nazionale delle Ricerche–Istituto Nazionale per la Fisica della Materia, Statistical Mechanics and Complexity, Dipartimento di Fisica, Sapienza–Università di Roma, P.le A. Moro 2, 00185 Roma, Italy. [5]Institute for Scientific Interchange Foundation, Viale S. Severo 65, 10133 Torino, Italy.

*To whom correspondence should be addressed. E-mail: stefano.zapperi@roma1.infn.it

displacement-controlled deformation, the driving stress decreases due to relaxation of the elastic strain. The total effective-stress drop caused by an avalanche of strain s is $(\Theta + \Gamma)s$, where Γ is the effective stiffness of the specimen-machine system (for a cubic compression specimen with rigid boundaries, Γ equals the elastic modulus E). This stress drop terminates the largest avalanches and, accordingly, we expect the cut-off to scale in inverse proportion with $(\Theta + \Gamma)$. A second scaling property can be motivated as follows: Large dislocation avalanches extend along a lamellar region across an entire specimen cross section. The total strain produced by such a "system-spanning" avalanche is proportional to the dislocation Burgers vector modulus b and inversely proportional to the characteristic specimen size L. Combining these relations, we find that [see also (*19*, *24*)]

$$s_0 \propto \frac{bE}{L(\Theta + \Gamma)} \tag{2}$$

To verify the validity of this scaling relation, we performed simulations of different system sizes in displacement control with a rigid constraint. As seen in Fig. 3, avalanche strain distributions obtained from specimens of different sizes fall on top of each other after rescaling $s \rightarrow S = sL(\Gamma + \Theta)/bE$ with $\Gamma = E$ and Θ deduced from the simulated stress strain curves (fig. S3). The same is true for the distribution we obtained under load control where $\Gamma = 0$, and we rescale by using the hardening coefficient Θ alone. The avalanche strain distributions obtained from our microbending simulations follow the same universal scaling curve if we identify L with the length of the bending beam and note that these simulations use displacement control.

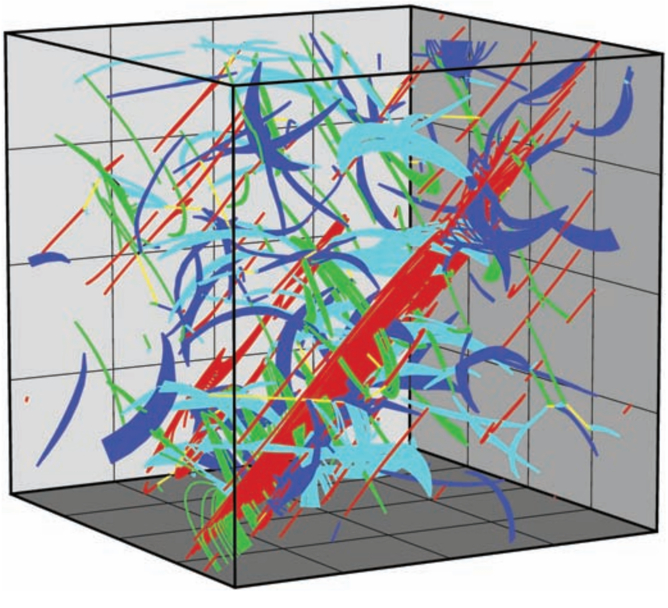

Fig. 2. Progress of a large dislocation avalanche in [010] symmetrical multiple slip for a specimen of size L = 0.5 μm. The graph shows an overlay of snapshots from every 10th global simulation timestep during a strain burst event. Red, green, blue, and cyan denote dislocations on the four {111} sets of crystal planes; yellow represents immobile Lomer locks created through dislocation reactions. Several geometrically separated dislocations become unpinned during the same event, which demonstrates the importance of long-range elastic interactions in strain burst initiation. The avalanche has a strongly anisotropic shape with more than 60% of the deformation occurring on one of the four equivalent sets of slip planes. Although a part of the deformation is taking place outside a single slip plane, the statistical analysis of the avalanche distribution suggests that the fractal dimension of the avalanches is close to two, indicating an effective lamellar shape.

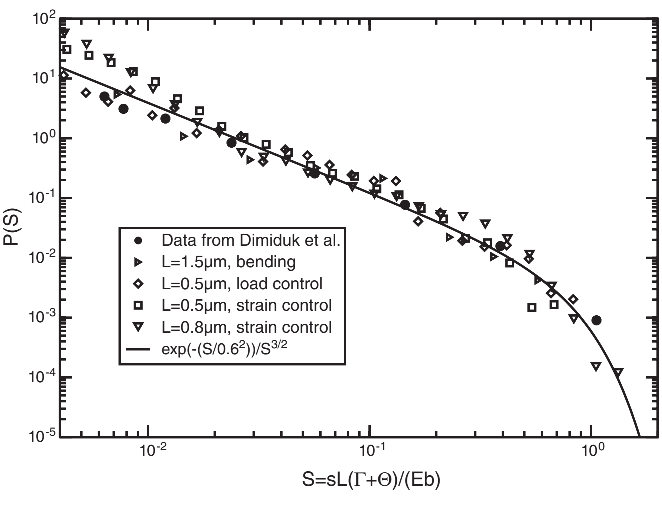

Fig. 3. Scaling collapse of avalanche size distributions. Open data points: data obtained from simulations of systems of different sizes in load and displacement control. Scaling parameters: $b = 2.8 \times 10^{-10}$ m (Al); $\Gamma = E$, $\Theta = E/10$ (displacement-controlled tension/compression and bending); $\Gamma = 0$, $\Theta = E/10$ (load-controlled tension/compression). Full data points: experimental data of Dimiduk *et al.* (*2*); scaling parameters: $b = 2.5 \times 10^{-10}$ m (Ni), $\Gamma = 0$, $\Theta = E/1000$ (load-controlled compression). Full line: scaling function $P(S) \propto S^{-3/2} \exp[-(S/0.6)^2]$.

It is instructive to apply the scaling (*2*) to the experimental data of (*2*) (solid circles in Fig. 3). In these experiments, the distribution of elongation increments $x = sL$ was determined during deformation in load control. Rescaling the experimental data points by setting $S = x\Theta/bE$ and using a hardening coefficient $\Theta = E/1000$ as deduced from the stress-strain curves in (*2*), we find that the scaled experimental data and simulation results are described by a single, universal scaling function, $P(S) \propto S^{-3/2} \exp[-(S/0.6)^2]$. In addition, the present theory can quantitatively explain high-resolution strain measurements that recorded strain bursts during stress-controlled torsion of tubular macroscopic samples of zinc, oriented for basal slip (*16*). Using the experimental parameters of (*16*), we estimate $s_0 \cong 2 \times 10^{-7}$, in agreement with the size of the largest strain jump reported in (*16*).

Our simulations demonstrate that intermittent dislocation avalanches are an intrinsic feature of crystal plasticity with properties that do not depend on the slip geometry, deformation mode, or details of the dynamical properties of dislocations. The avalanches are statistically characterized by a universal probability distribution whose characteristic parameter s_0 is determined by the specimen size, the hardening capacity of the material, and the response of the deformation "machine" to an avalanche. But what are the implications of these findings for deformation processes on the micrometer scale? To elucidate this aspect, we performed stochastic simulations of the bending of a long thin rod subjected to a bending moment that is constant along its length. The basic idea of these simulations (*19*) is that a long thin rod can be considered as a chain of segments that are similar to those we have simulated by discrete dislocation dynamics, and that behave in a statistically independent manner. The applied bending moment is increased until the total bending angle exceeds 2π, when the rod should assume an annular shape. As a consequence of the stochastic and intermittent nature of the deformation process, the deformation behavior of the individual segments can, however, no longer be predicted in a deterministic sense. As the maximum avalanche strain increases with decreasing system size, the stochastic heterogeneity of deformation becomes more and more pronounced. This leads to irregular shape distortions, as shown in Fig. 4. In the limit of very thin rods (illustrated by the bottom right shape in Fig. 4), the stochastic heterogeneity does not increase further: In very small specimens, the largest strain bursts that occur before the simulation is terminated remain below the intrinsic cut-off s_0 of the probability distribution.

Our findings demonstrate that it may be difficult, on the micrometer and submicrometer scale, to control the results of plastic-forming processes. Note, however, that micrometer-scale components such as bonding wires that are processed through plastic forming are polycrystals. We have studied the influence of grain boundaries on the propagation of dislocation avalanches by simulating bicrystalline and multicrystalline samples (*19*). The results suggest that in polycrystals, grain bounda-

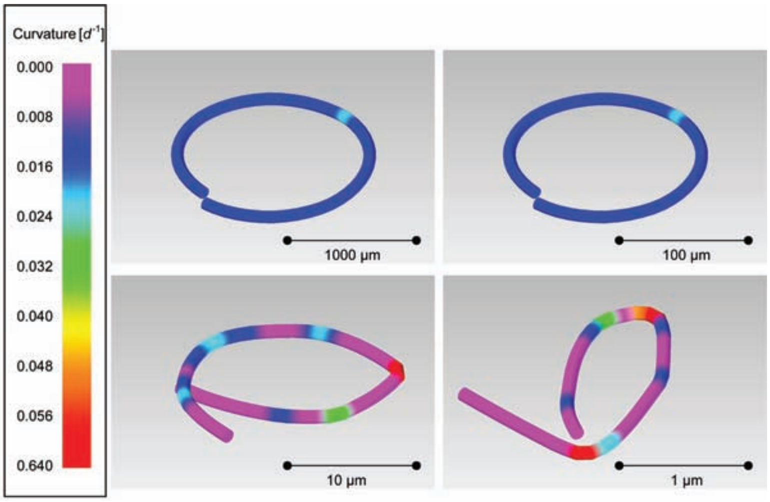

Fig. 4. Shapes of rods (aspect ratio 1:50) after simulated bending; rod thickness t from top left to bottom right: t = 100 µm, t = 10 µm, t = 1 µm, t = 0.1 µm; $b = 2.8 \times 10^{-10}$ m, $\Theta = E/1000$; the color code indicates the local bending angle over a segment of length t. In the last rod, the maximum avalanche size occurring in the simulations falls below the intrinsic cut-off of the distribution.

ries hinder avalanche propagation (fig. S4), and thus the size of strain bursts is reduced by a factor of $(\xi/L)^2$, where ξ is the grain size [see (*19*) for a more detailed discussion]. Accordingly, formability may be ensured even on the submicrometer scale if a correspondingly small grain size can be maintained throughout the processing.

Our results demonstrate the universality of avalanche behavior in plasticity and elucidate the crossover between intermittent and smooth plastic flow. That avalanche strains decrease in inverse proportion to sample size explains why it is difficult to observe strain bursts in macroscopic samples. In AE measurements, by contrast, the acoustic energy is recorded. The acoustic energy release during a dislocation avalanche may be assumed to be proportional to the dissipated energy e, which is related to the strain s by $e \approx \sigma s V$, where σ is the stress and V is the volume. Hence, the cutoff of the AE energy distribution is expected to increase with sample size as $e_0 \propto L^2$. This explains why acoustic emission avalanches are observed in macroscopic single crystals, whereas strain avalanches are not.

The picture that emerges from our analysis indicates that, even though the phenomenology of plastic deformation changes markedly with decreasing sample size, the fundamental physical processes are the same in macroscopic and micrometer-scale specimens. Dislocation avalanches on all scales arise from the most basic features of dislocation motion and can be described by a generic statistical distribution. In single crystals, the largest dislocation avalanches extend across an entire cross section of the specimen: Their extension is limited only by the sample size, and the stochastic nature of their occurrence may make it impossible to control the shapes resulting from a deformation process. In polycrystals, by contrast, dislocation avalanches are limited by grain boundaries. This may lead to an appreciable smoothing of deformation and improve the controllability of deformation processes.

References and Notes

1. M. D. Uchic, D. M. Dimiduk, J. N. Florando, W. D. Nix, *Science* **305**, 986 (2004).
2. D. M. Dimiduk, C. Woodward, R. LeSar, M. D. Uchic, *Science* **312**, 1188 (2006).
3. M. C. Miguel, A. Vespignani, S. Zapperi, J. Weiss, J. R. Grasso, *Nature* **410**, 667 (2001).
4. J. Weiss, J. R. Grasso, *J. Phys. Chem. B* **101**, 6113 (1997).
5. J. Weiss, F. Lahaie, J. R. Grasso, *J. Geophys. Res.* **105**, 433 (2000).
6. J. Weiss, D. Marsan, *Science* **299**, 89 (2003).
7. T. Richeton, J. Weiss, F. Louchet, *Nat. Mater.* **4**, 465 (2005).
8. T. Richeton, P. Dobron, F. Chmelik, J. Weiss, F. Louchet, *Mater. Sci. Eng. A* **424**, 190 (2006).
9. J. Schwerdtfeger *et al., J. Stat. Mech.* L04001 (2007).
10. L. P. Kubin, C. Fressengeas, G. Ananthakrishna, in *Dislocations in Solids*, F. R. N. Nabarro, M. S. Duesbery, Eds. (North-Holland, Amsterdam, 2002), vol. 11, p. 101.
11. J. P. Sethna, K. A. Dahmen, C. R. Myers, *Nature* **410**, 242 (2001).
12. G. Durin, S. Zapperi, in *The Science of Hysteresis*, G. Bertotti, I. Mayergoyz, Eds. (Academic Press, New York, 2005), p. 181; also available at http://arxiv.org/abs/cond-mat/0404512.
13. E. V. Colla, L. K. Chao, M. B. Weissman, *Phys. Rev. Lett.* **88**, 017601 (2002).
14. A. Petri, G. Paparo, A. Vespignani, A. Alippi, M. Costantini, *Phys. Rev. Lett.* **73**, 3423 (1994).
15. L. I. Salminen, A. I. Tolvanen, M. J. Alava, *Phys. Rev. Lett.* **89**, 185503 (2002).
16. R. F. Tinder, J. P. Trzil, *Acta Metall.* **21**, 975 (1973).
17. H. H. Potthoff, *Phys. Stat. Sol. (a)* **77**, 215 (1983).
18. H. Godon, H. H. Potthoff, H. Neuhauser, *Cryst. Lattice Defects* **19**, 373 (1984).
19. See supporting material available on *Science* Online.
20. D. Weygand, L. H. Friedman, E. van der Giessen, A. Needleman, *Model. Simul. Mater. Sci. Eng.* **10**, 437 (2002).
21. D. Weygand, P. Gumbsch, *Mat. Sci. Eng. A* **400-401**, 158 (2005).
22. M. Zaiser, P. Moretti, *J. Stat. Mech.* P08004 (2005).
23. M. Zaiser, *Adv. Phys.* **55**, 185 (2006).
24. M. Zaiser, N. Nikitas, *J. Stat. Mech.* P04013 (2007).
25. Financial support of the European Commissions Human Potential Programme SizeDepEn (contract MRTN-CT-2003-504634) and the New and Emerging Science and Technologies (NEST) Pathfinder program Triggering Instabilities in Materials and Geosystems (contract NEST-2005-PATH-COM-043386), as well as by the Engineering and Physical Science Research Council (grant EP/E029825), is gratefully acknowledged. Part of this work was performed on the PC cluster of the Department of Theoretical Physics at Eötvös University and at the High Performance Computing calculation facilities of the Rechenzentrum, University of Karlsruhe, within the HPC_DDD project. C.M. acknowledges the financial support of the Austrian Fonds zur Förderung der wissenschaftlichen Forschung (FWF) through project J2646-N13. D.W. acknowledges the financial support of the European Union project NMP3-CT-2006-016710 (NANOMESO).

Supporting Online Material

www.sciencemag.org/cgi/content/full/318/5848/251/DC1
SOM Text
Figs. S1 to S4
References

12 April 2007; accepted 17 August 2007
10.1126/science.1143719

Polymers with Cavities Tuned for Fast Selective Transport of Small Molecules and Ions

Ho Bum Park,[1,2] Chul Ho Jung,[1] Young Moo Lee,[1*] Anita J. Hill,[3] Steven J. Pas,[3] Stephen T. Mudie,[3] Elizabeth Van Wagner,[2] Benny D. Freeman,[2] David J. Cookson[4]

Within a polymer film, free-volume elements such as pores and channels typically have a wide range of sizes and topologies. This broad range of free-volume element sizes compromises a polymer's ability to perform molecular separations. We demonstrated free-volume structures in dense vitreous polymers that enable outstanding molecular and ionic transport and separation performance that surpasses the limits of conventional polymers. The unusual microstructure in these materials can be systematically tailored by thermally driven segment rearrangement. Free-volume topologies can be tailored by controlling the degree of rearrangement, flexibility of the original chain, and judicious inclusion of small templating molecules. This rational tailoring of free-volume element architecture provides a route for preparing high-performance polymers for molecular-scale separations.

Small-molecule and ion diffusion through cavities (i.e., free-volume elements) in soft organic materials is an inherently subnano- or nanoscopic phenomenon. It has important implications for membrane separation processes in chemicals production as well as energy conver-

Science

Dislocation Avalanches, Strain Bursts, and the Problem of Plastic Forming at the Micrometer Scale

Ferenc F. Csikor, Christian Motz, Daniel Weygand, Michael Zaiser and Stefano Zapperi

Science **318** (5848), 251-254.
DOI: 10.1126/science.1143719